Annales Societatis Geologorum Poloniae (2016), vol. 86: 249–264. doi: http://dx.doi.org/10.14241/asgp.2016.014

WEATHERING IN A REGOLITH ON THE WERENSKIOLDBREEN FOREFIELD (SW SPITSBERGEN): MODELLING OF PORE WATER CHEMISTRY

Monika KWAŚNIAK-KOMINEK[1], Maciej MANECKI[1], Grzegorz RZEPA[1], Anna M. PŁONKA[2] & Dorota GÓRNIAK[3]

[1] AGH University of Science and Technology, Faculty of Geology, Geophysics and Environmental Protection, al. Mickiewicza 30, 30-059, Kraków, Poland; e-mail: monika.kwasniak@gmail.com, gpmmanec@cyf-kr.edu.pl, gprzepa@cyf-kr.edu.pl

[2] Yeshiva University, Department of Physics, New York 10033, United States; e-mail: anna.plonka@yu.edu

[3] University of Warmia and Mazury in Olsztyn, Department of Microbiology, ul. Oczapowskiego 1a, 10-957 Olsztyn, Poland; e-mail: gorniak@uwm.edu.pl

Kwaśniak-Kominek, M., Manecki, M., Rzepa, G., Płonka, A. M. & Górniak, D., 2016. Weathering in a regolith on the Werenskioldbreen forefield (SW Spitsbergen): modelling of pore water chemistry. *Annales Societatis Geologorum Poloniae*, 86: 249–264.

Abstract: The mineral framework and pore waters of glacial sediments exposed in the foreland of Werenskioldbreen in SW Spitsbergen were sampled and analyzed to model the evolution of pore water chemistry, representing the advancement of weathering in a chronosequence. Three samples were taken at distances representing snapshots of approximately 5, 45 and 70 years of exposure. Complementary mineralogical analyses of the mineral framework and chemical analyses of pore waters, coupled with thermodynamic modelling of mineral-water interactions were applied. Recently uncovered sediments of the bottom moraine underwent very little weathering underneath the glacier cover; both the sediments and pore waters in the forefield of the Werenskioldbreen represent a very immature system. Poorly sorted sediments were deposited by the glacier and not reworked by fluvioglacial waters. The ratio of 'amorphous iron' to 'free iron' Fe_o/Fe_d increases with distance from the glacier terminus from 0.30 through 0.36 to 0.49, typical for fresh glacial till. The increase in saturation with CO_2 (from $p(CO_2)$ –3.8 to –2.4) and the concentration of all major ions in pore waters (from 123 to 748 mg/L total dissolved solids, TDS) was observed in this young chronosequence. The waters evolved from carbonate-dominated to sulphate-dominated, indicating that with progress in weathering the dominating processes are equilibration with carbonates, oxidation of sulphides and the influence of gypsum precipitation by seasonal freeze-thaw cycles. Mass balance calculations and inverse modelling of the composition of pore waters, verified by microscopic observations of alteration on the surfaces of mineral grains, allowed thermodynamic confirmation of the fact that the relative significance of carbonate weathering decreases and that of sulphate increases down the chronosequence. The participation of silicate minerals in weathering is low, indicating a relatively immature stage of weathering within this particular chronosequence. It is significant that the morphology of etch pits and the formation of secondary phases apparent on mineral surfaces were identical, regardless of the distance from the glacier terminus. This might indicate that the mechanisms of particular weathering processes at the mineral-water interface are the same at the initial as well as at the more mature stages and do not change at least within ca. 70 years of exposure.

Key words: Retreating glaciers, chronosequence, hydrochemistry, Werenskioldbreen, Spitsbergen.

Manuscript received 23 November 2015, accepted 24 August 2016

INTRODUCTION

The continuous and relatively fast retreat of many glaciers noted worldwide is particularly pronounced in the highly sensitive polar systems in the Arctic (Jania and Hagen, 1996; Hodson *et al.*, 2000; Tranter *et al.*, 2002; Anderson, 2007; Wadham *et al.*, 2007; Bernasconi *et al.*, 2008; Straneo and Heimbach, 2013). In the foreland of retreating glaciers, recently uncovered glacigenic sediments and regolith are exposed to atmospheric conditions and undergo rapid weathering, resulting in the formation of initial polar soils (Anderson *et al.*, 1997, 2000; Huggett, 1998). This sets

the scene for studies of the evolution of the system in chronosequences. Classical studies of chronosequences in front of retreating glaciers are best known from the Alps and Alaska (see Bernasconi *et al.*, 2008; Dümig *et al.*, 2011; Dahms *et al.*, 2012 for a recent literature review). Recently, studies of glacier forelands have also received attention in Svalbard (Wadham *et al.*, 1997, 2001; Cooper *et al.*, 2002, 2011; Hodgkins *et al.*, 2009; Bradley *et al.*, 2014). The character of the glaciers in Svalbard, which often form networks and ice caps, differs significantly from contemporary glaciers in the Alps and resembles the ice cover in the Alps during glaciation periods. Therefore, the retreat of the Svalbard glaciers can be used as a proxy for deglaciation processes in Northern Europe after glaciation periods in the past.

The dominating processes in the early stages of weathering in the polar climate are dissolution of carbonates and oxidation of sulphides (Anderson *et al.*, 1997, 2000; Bukowska-Jania, 2007; Kabała and Zapart, 2009). At more mature stages, after most of the carbonate and sulphide are leached from the soils, silicate dissolution and transformation become important (Taylor and Blum, 1995; Anderson *et al.,* 1997, 2000). Both steps are associated with microbial activity (Huggett, 1998; Anderson, 2007). While the initial stages are dominated by dissolution and removal, more advanced weathering is characterized by the formation of secondary phases.

The mechanisms and rates of dissolution and transformations for rock-forming minerals are relatively well known (e.g., Churchman, 2000; Brantley, 2003; White, 2003; Wilson, 2004; Zhu, 2005 and the literature cited therein). The formation of young polar soils also has been described before (Huggett, 1998; Kabała and Zapart, 2009). However, discrepancies between laboratory and field results are often apparent (White and Brantley, 2003). They result partly from the processes inherent to the weathering of silicate minerals (e.g., evolution of roughness) and partly from extrinsic parameters (e.g., high mineral/fluid ratio, low permeability, and high solute concentrations). As a consequence, highly unsaturated systems are created in laboratory experiments, while conditions close to thermodynamic equilibrium are observed in the field. According to Alexander and Burt (1996), about 10 years is necessary for observation of the beginning of the alteration process in soils after deglaciation. However, the present authors observed the advanced dissolution of carbonates and the oxidation of pyrite in samples exposed for less than 5 years. There is no doubt that more knowledge is needed about the initial stages of weathering, particularly at the microscopic level, as they are different from the general bulk characteristics of chemical weathering in polar soils.

Werenskioldbreen, a glacier located near the SW coast of Spitsbergen, is an excellent model system for studies of the weathering patterns in the foreland of a retreating glacier. It has been retreating since the beginning of the XX century, with an average velocity of 25 m/year (Bukowska-Jania, 2003). The geography, geology and hydrology of the area are relatively well known. The glacier itself is similar to many other retreating glaciers in Svalbard, indicating that the processes described here are quite typical for this part of the Arctic. Furthermore, the diverse metamorphic geology of the catchment provides a variety of major and accessory rock-forming minerals, including all major carbonates present in the environment studied, which allows for a broad and relatively universal approach.

Weathering processes and the evolution of the initial soil in the area, recently uncovered by the retreating glaciers, is strongly biologically affected. The role of microbes in the mediation of weathering in polar soil systems is widely recognized (Sigler and Zeyer, 2002; Nemergut *et al.,* 2007; Yoshitake *et al.,* 2007). However, biological effects on weathering cannot be fully appreciated without an in-depth knowledge of the inorganic, geochemical processes governing the system. The objective of this study is the semi-quantitative characterization of inorganic mineral-water interaction processes in the chronosequence of Werenskioldbreen. This provides a background for a microbial study, presented in the second part of the contribution (in preparation).

To date, most publications dealing with the foreland of Werenskioldbreen or similar retreating glaciers have been focused on the glacier itself (Bukowska-Jania and Jania, 1988), the soils (Kabała and Zapart, 2009, 2012), or characterization of the composition of surface waters (Anderson *et al.*, 1997; Bukowska-Jania, 2007; Wadham *et al.*, 2007; Krawczyk *et al.*, 2008). Generally, for very young systems dominated by carbonate and sulphate ions, the chemical analyses of surface waters represent the system well. However, the present authors observed an increase of soil pore water mineralization with distance from glacier terminus. This pattern is the opposite of what is observed in surface waters running, for example, in the foreland of the Bench Glacier in Alaska (Anderson *et al.*, 2000). Therefore, the current investigation focuses on the correlation of pore water composition and microscopic scale *in-situ* observation of mineral transformations with thermodynamic models of mineral-water reactions. The authors believe that a solely macroscopic approach (determination of the average mineral composition of regolith or the average chemical composition of running waters, etc.) is insufficient for an explanation of the mechanisms of the processes observed. The computer modelling of specific reactions, verified by field and microscopic observations, is applied here to determine, model, and quantify the effect of dissolution and transformations of particular minerals on the composition of pore waters. This way, thermodynamic calculations, rather than qualitative speculations, can be used to identify the key reactants in particular stages of the evolution of this system in an attempt to explain the reasons for and the mechanisms of pore water evolution in a young proglacial sediment, affected by the initial stages of weathering. This knowledge will help an understanding of the mechanisms of initial soil formation, necessary for characterization of the microbial succession along the chronosequences in the Arctic.

STUDY AREA

The Werenskioldbreen is located in Wedel Jarlsberg Land, near the SW coast of West Spitsbergen (Fig. 1). It is a

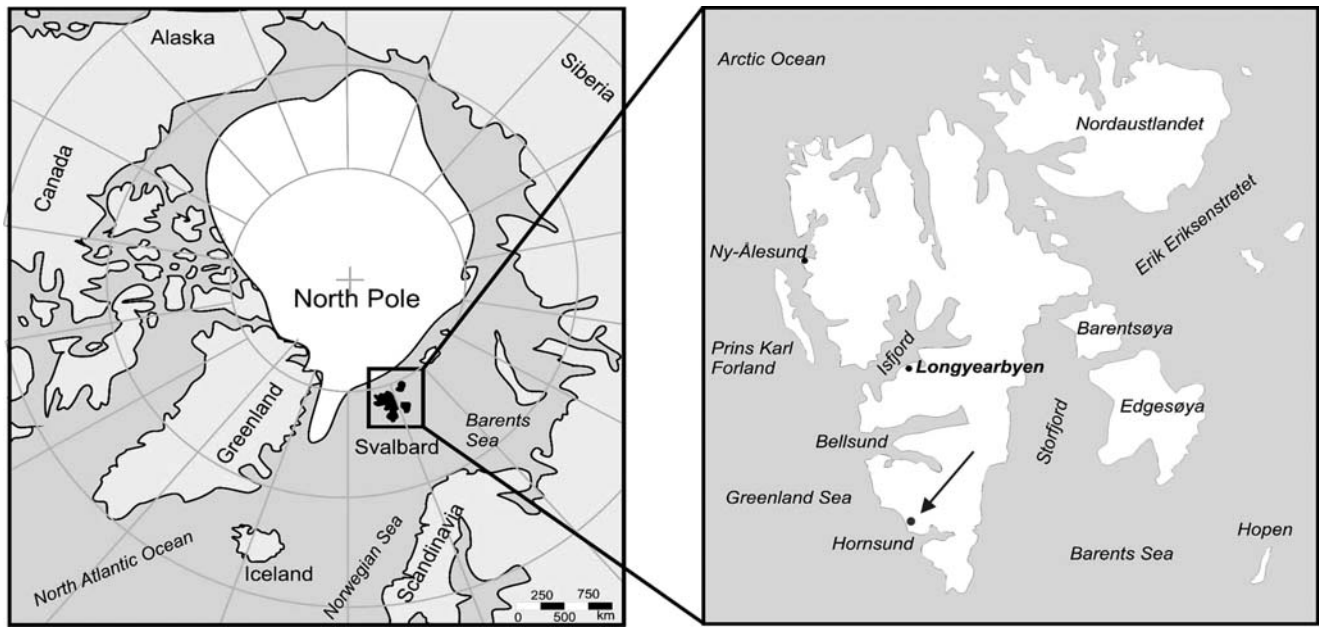

Fig. 1. Location of Svalbard in High Arctic. Summer sea ice cover in Arctic is approximated. The arrow indicates the position of Werenskioldbreen.

27 km^2 subpolar polythermal glacier, which terminates on land (Pälli *et al.*, 2003). The area is under the influence of a suboceanic Arctic climate, with an average annual temperature of –4.4 °C and precipitation of 430 mm (Marsz and Styszyńska, 2007). The relatively flat proglacial zone of the glacier is surrounded by elevated lateral and terminal moraines. The moraines are only locally covered with soils. Soils currently forming in the forefield of the Werenskioldbreen are in the initial stage of development. According to Skiba *et al.* (2002), these soils have poorly developed horizons, due to an excessive frost-induced mixing of the surface layer and the low intensity of mineral weathering. The soils thaw in summer and the permafrost layer starts at a depth of ca. 100 cm below ground level (Kabała and Zapart, 2012). The till, in most cases, is structureless in the pedological sense, often greenish grey and gleyed, owing to continuous saturation with water (Kabała and Zapart, 2009).

The geology of this area was summarized and described in detail by Czerny *et al.* (1993). The rocks covered by the Werenskioldbreen consist of a metasedimentary-metavolcanic polymetamorphic sequence, probably Mesoproterozoic in age of the protolith. The succession includes mostly the Deilegga Formation, the Eimfjellet Formation, the Jens Erikfjellet Formation and the Vimsodden Formation and was subjected to amphibolite facies metamorphism in the Late Cryogenian (ca. 640 Ma), which was followed by greenschist facies Caledonian metamorphism (Manecki *et al.*, 1998; Majka *et al.*, 2008, 2010, 2013). A major regional dislocation zone cuts across underneath the glacier from Vimsodden through Kosibapasset (Czerny *et al.*, 1992a). The variable lithology consists mostly of phyllites, carbonate- and quartz-carbonate-mica schists, chlorite schists, conglomerates, amphibolites, greenschists, and marbles. The carbonate minerals include calcite, dolomite, ankerite, and siderite. Polymetallic mineralization layers with Fe, Cu, Pb and Zn sulphides are locally apparent along the dislocation zone (Czerny *et al.*, 1992b; Kieres and Piestrzyński, 1992).

MATERIALS AND METHODS

Three soil and pore water samples were collected from the southern part of the glacier forefield (Fig. 2). The sample locations, which in 2005 were 20 m (sample C), 950 m (sample M), and 1700 m (sample F) from the glacier terminus, were chosen to compare the progression of weathering

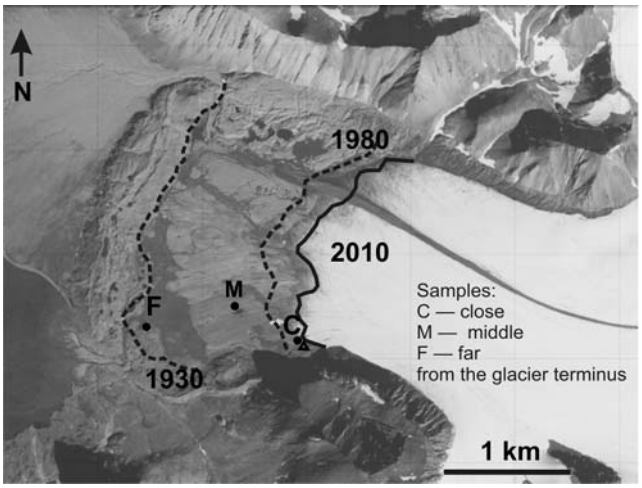

Fig. 2. Location of sampling sites in the forefield of Werenskioldbreen, which in 2010 were 20 m (C – close to the glacier terminus), 950 m (M – middle distance from the glacier terminus), and 1700 m (F – far from the glacier terminus). A triangle marks location of glacial runoff sampling site. Topography after orthophotomap (Kolondra, 2002). Position of glacier terminus compiled from literature and observations (Bukowska-Jania and Jania, 1988).

Table 1

Weathering processes included in the mass balance modelling

Sea salt input is not included in the reactions
Dissolution of carbonates Calcite $CaCO_3 = Ca^{2+} + CO_3^{2-}$ Dolomite $CaMg(CO_3)_2 = Ca^{2+} + Mg^{2+} + 2\ CO_3^{2-}$ Siderite $Fe_{0.7}Mn_{0.3}CO_3 = 0.7\ Fe^{2+} + 0.3\ Mn^{2+} + CO_3^{2-}$
Sulphate from sulphide oxidation $FeS_2 + 3.75\ O_2 + 2\ H_2O = 2\ SO_4^{2-} + 4\ H^+ + 0.5\ Fe_2O_3$
Weathering of aluminosilicates and silicates: Albite $NaAlSi_3O_8 + 8\ H_2O = Na^+ + Al(OH)_4^- + 3\ H_4SiO_4$ Bbiotite $KFeMg_2AlSi_3O_{10}(OH)_2 + 6\ H^+ + 4\ H_2O = K^+ + Fe^{2+} + 2\ Mg^{2+} + Al(OH)_4^- + 3\ H_4SiO_4$ Hornblende $KNaCa_{1.5}Al_3Mg_4Si_6O_{22}(OH)_2 + 22\ H^+ = K^+ + Na^+ + 1.5\ Ca^{2+} + 3\ Al^{3+} + 4\ Mg^{2+} + 6\ H_4SiO_4$ K-feldspar $KAlSi3O8 + 8\ H_2O = K^+ + Al(OH)_4^- + 3\ H_4SiO_4$ Plagioclase $Na_{0.62}Ca_{0.38}Al_{1.38}Si_{2.62}O_8 + 5.52\ H^+ + 2.48\ H_2O = 0.62\ Na^+ + 0.38\ Ca^{2+} + 1.38\ Al^{3+} + 2.62\ H_4SiO_4$ Chlorite $Fe_2Mg_3Al_2Si_3O_{10}(OH)_8 + 16\ H^+ = 2\ Fe^{2+} + 3\ Mg^{2+} + 2\ Al^{3+} + 3\ H_4SiO_4 + 6\ H_2O$
Precipitation of secondary minerals: Goethite $FeOOH + 3\ H^+ = Fe^{3+} + 2\ H_2O$ Illite $K_{0.6}Mg_{0.25}Al_{2.3}Si_{3.5}O_{10}(OH)_2 + 11.2\ H_2O = 0.6\ K^+ + 0.25\ Mg^{2+} + 2.3\ Al(OH)_4^- + 3.5\ H_4SiO_4 + 1.2\ H^+$ Kaolinite $Al_2Si_2O_5(OH)_4 + 6\ H^+ = H_2O + 2\ H_4SiO_4 + 2\ Al^{3+}$ Ca-montmorillonite $Ca_{0.165}Al_{2.33}Si_{3.67}O_{10}(OH)_2 + 12\ H_2O = 0.165\ Ca^{2+} + 2.33\ Al(OH)_4^- + 3.67\ H_4SiO_4 + 2\ H^+$

with the time of exposure from under the glacier. The approximate age of exposure (about 5, 45, and 70 years, respectively) was assessed on the basis of the history of retreat recorded in the literature (Bukowska-Jania and Jania, 1988; Kabała and Zapart, 2009, and the literature cited therein). More detailed sampling was not possible during the time of the expedition for technical reasons. Sampling was at sites, which do not show reworking by fluvial waters. The areas where sample sites were chosen differ from each other in the extent of surface maturity, the amount of patchy vegetation, and the initial soil development as characterized by Kabała and Zapart (2009), which indicates that these sites are representative of the chronosequence. The samples for analysis (ca. 3 kg) represent the average composition from a depth of 0–30 cm. The particle-size distribution of the coarser fraction (>2 μm) was determined by wet sieving. The clay fraction (<2 μm) was separated by gravity settling in distilled water. No saturation with K or Mg was applied. The heavy-mineral fraction was separated, using heavy liquid $C_2H_2Br_4$ (density 2.96 g/cm^3).

The mineral composition of the soils was determined by petrographic microscopy in polarized light, X-ray diffractometry and scanning electron microscopy. Petrographic thin sections were prepared, using the fraction of 0.02–0.5 mm by mixing with epoxy resin. Powder X-ray diffraction (XRD) was used for the identification of clays. For X-ray diffraction, a Philips PW 3020 X'Pert-APD diffractometer was used (Cu radiation, graphite monochromator, steps of 0.05 °2Θ in 3–70° range). Separation of the clay fraction (<2 μm) was accomplished by wet sieving, followed by settling. Oriented specimens were prepared by gravity sedimentation of clay onto glass slides (surface density 10 mg/cm^2). The characterization of clay minerals requires that a variety of treatments be performed on each <2 μm specimen. Three diffractograms were routinely acquired using oriented mounts of each sample that were air dried, ethylene glycol solvated, and heat treated at 550 °C for 5 hr.

The mechanisms and products of mineral transformations were examined using an environmental scanning electron microscope (FEI QUANTA 200 FEG), equipped with an EDS spectrometer (EDAX). Mineral surfaces were imaged in low vacuum without coating. The grains were separated by hand from the 0.5 mm fraction using a stereoscopic Olympus SZX–9 microscope. The combined application of stereoscopic microscope and SEM-EDS allowed for the identification of minerals, based on morphology, colour, cleavage, and element composition.

The maturity of soils was assessed on the basis of the 'amorphous' to 'free iron' ratio Fe_o/Fe_d. This ratio has been called an 'activity ratio' and has been used as a relative measure of the crystallinity of secondary iron oxides (Schwertmann, 1985). Fe_o is the amount of iron leached from soil using acid ammonium oxalate, according to Tamm's method (Van Reeuwijk, 2006). Fe_d is the amount of iron leached from soil using the bicarbonate-dithionite-citrate method, according to Mehra and Jackson (Mehra and Jackson, 1960; Van Reeuwijk, 2006). Each time, 0.2 g of pulverized soil was used with 100 mL of leaching solution. The concentration of Fe in solution was determined using a Philips PU-9100x AAS spectrometer and applying Merck standards, diluted in a matrix of extracting solutions. The results are the averages of duplicated analyses.

Samples of pore waters were collected along with sediment at the very same localities by filtering pore water, which drained by gravity into holes in the ground 30 cm deep. All three samples were collected in July 2010 at the same time under the same hydrologic conditions. Simultaneously, a sample of water was taken from a creek 1.5 m wide and 0.2 m deep, very close to the glacier terminus (Fig. 2). This is one of the main glacier outlet streams on the southernmost side of the central moraine. Electrolytic conductivity, pH, Eh, and oxygen content were measured in the field. The water was filtered in the field through 0.2 μm PC membranes into high-density polyethylene (HDPE) bottles:

Table 2

Selected reactions and constants used for modification of PHREEQC thermodynamic database

Phase		log K	ΔH
Calcite	$CaCO_3 = CO_3^{2-} + Ca^{2+}$	–8.48	–2.297
Dolomite	$CaMg(CO_3)_2 = Ca^{2+} + Mg^{2+} + 2\ CO_3^{2-}$	–17.09	–9.436
Siderite	$Fe_{0.7}Mn_{0.3}CO_3 = 0.7\ Fe^{2+} + 0.3\ Mn^{2+} + CO_3^{2-}$	–10.89	–2.480
K-feldspar	$KAlSi_3O_8 + 8\ H_2O = K^+ + Al(OH)_4^- + 3\ H_4SiO_4$	–20.57	30.820
Albite	$NaAlSi_3O_8 + 8\ H_2O = Na^+ + Al(OH)_4^- + 3\ H_4SiO_4$	–18.00	25.896
Anorthite	$CaAl_2Si_2O_8 + 8\ H_2O = Ca^{2+} + 2\ Al(OH)_4^- + 2\ H_4SiO_4$	–19.71	11.580
Plagioclase	$Na_{0.62}Ca_{0.38}Al_{1.38}Si_{2.62}O_8 + 5.52\ H^+ + 2.48\ H_2O = 0.62\ Na^+ + 0.38\ Ca^{2+} + 1.38\ Al^{3+} + 2.62\ H_4SiO_4$	14.10	
Biotite	$KAlMg_3Si_3O_{10}(OH)_2 + 10\ H^+ = Al^{3+} + K^+ + 3\ Mg^{2+} + 3\ H_4SiO_4$	37.44	–74.16
Pyrite	$FeS_2 + 2\ H^+ + 2\ e^- = Fe^{2+} + 2\ HS^-$	–18.48	11.300
Chlorite	$Fe_2Mg_3Al_2Si_3O_{10}(OH)_8 + 16\ H^+ = 2\ Fe^{2+} + 3\ Mg^{2+} + 2\ Al^{3+} + 3\ H_4SiO_4 + 6\ H_2O$	68.38	–151.49
Hornblende	$KNaCa_{1.5}Al_3Mg_4Si_6O_{22}(OH)_2 + 22.0\ H^+ = K^+ + 1.0\ Na^+ + 1.5\ Ca^{2+} + 3.0\ Al^{3+} + 4.0\ Mg^{2+} + 6.0\ H_4SiO_4$	101.99	–880.205
Kaolinite	$Al_2Si_2O_5(OH)_4 + 6\ H^+ = H_2O + 2\ H_4SiO_4 + 2\ Al^{3+}$	7.43	–35.300
Illite	$K_{0.6}Mg_{0.25}Al_{2.3}Si_{3.5}O_{10}(OH)_2 + 11.2\ H_2O = 0.6\ K^+ + 0.25\ Mg^{2+} + 2.3\ Al(OH)_4^- + 3.5\ H_4SiO_4 + 1.2\ H^+$	–40.27	54.684
Ca-montmorillonite	$Ca_{0.165}Al_{2.33}Si_{3.67}O_{10}(OH)_2 + 12\ H_2O = 0.165\ Ca^{2+} + 2.33\ Al(OH)_4^- + 3.67\ H_4SiO_4 + 2\ H^+$	–45.03	58.37
Pyrolusite	$MnO_2{\cdot}H_2O + 4\ H^+ + 2\ e^- = Mn^{2+} + 3\ H_2O$	41.38	–65.110
Goethite	$FeOOH + 3\ H^+ = Fe^{3+} + 2\ H_2O$	–1.00	

one portion of each sample was acidified with concentrated HNO_3. Major cations and anions as well as manganese, nitrate and silica were determined in the field in non-acidified samples using the HACH 2800 spectrophotometer with HACH standard tests. Acidified samples were taken back to Poland for the determination of trace element and the verification of field results. Flame emission spectrometry was used for K and Na. Alkalinity, Ca, Mg, and Cl were determined by titration, while F was measured using colourimetry (HITACHI U–1800 UV-vis spectrophotometer). The concentration of Al, Sr, and Li ions was determined by ICP-OES. All analyses were completed within 6 months of sample collection. The charge balance of the analyses, defined as 100 × (Σcations – Σanions) / (Σcations + Σanions), where concentrations are expressed in meq/L, is below 7%.

The mineral-water interactions responsible for the evolution of pore water composition were simulated using mass balance calculation by inverse modelling in the PHREEQC computer code (Parkhurst, 1995). The minerals and weathering reactions included in the model are presented in Table 1. The reactions involve dissolution and precipitation, redox processes, and ion exchange. A modified PHREEQC database provided with the code was used in the modelling. Selected reactions and constants used for modification of the database are presented in Table 2. The models were used for ionic speciation of the solutions, followed by the projection of the results on stability diagrams, as well as for inverse modelling of the reaction pathways.

COMPOSITION OF THE REGOLITH

The grain-size distribution (Fig. 3) is comparable to those of Bukowska-Jania (2003) and Kabała and Zapart (2009, 2012). The sediments consist primarily of gravel, sand, and silt, which are typical for moraine deposits. The clay content is below 4 wt.%. The sample taken closest to the glacier front exhibits the lowest sand content and the highest gravel content. All these sediments were transported and deposited by the glacier and not reworked by fluvioglacial waters. Therefore, the grain-size distribution results from the fact that the base material is largely mixed and composed partly of ground moraine till and sandur, and partly of lateral moraine, consistent with observations by Bukowska-Jania (2003).

One of the useful indicators of the intensity of weathering of primary minerals and the advance of pedogenesis is the ratio of "amorphous" iron to "free" iron Fe_o/Fe_d (Schwertmann, 1985). Normally, in fresh glacial till this ratio amounts to <0.5 (Alexander and Burt, 1996). The values of

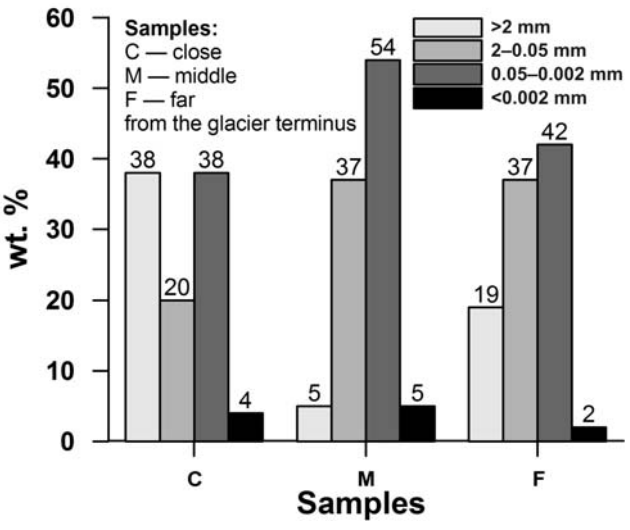

Fig. 3. Grain-size distribution. Sample symbols as in Figure 2.

Table 3

Semi-quantitative mineral composition of sediments

Sample	C	M	F
Distance from glacier terminus	20 m	950 m	1700 m
Quartz	+++	+++	+++
Calcite	++	++	++
Dolomite	++	++	++
Siderite Snkerite	+ +	++	+
Biotite	+	+	+
Hornblende	++	++	++
Plagioclase	++	++	++
Chlorite			++
Muscovite 2M1	+	+	+
Amphibole	+	+	
Pyrite	+	+	+
Goethite	+	+	+
Mica-vermiculite			+
Mica-smectite			+
Smectite-illite		+	

(+++) – frequent mineral, (++) – common mineral, (+) – accessory mineral

Fe_o determined in the soil samples equal to 290 ppm in C, 580 ppm in M, and 560 ppm in the oldest sample F. Similarly, Fe_d equals 970 ppm, 1620 ppm, and 1140 ppm in C, M, and F, respectively. Accordingly, the Fe_o/Fe_d ratios measure 0.30 for C, 0.36 for the M sample and 0.49 for the F sample. As expected, the Fe_o/Fe_d ratio increases with the age of the soils. A similar pattern was observed by Kabała and Zapart (2009).

Minerals identified in the sediments analyzed are listed in Table 3. The quantitative determination of the mineral composition of the regolith is unnecessary for the purpose of modelling. The approach presented here stems from the fact that the importance of a mineral component in the system is reflected not by the total amount present, but by the total amount involved in the reactions (in moles of mineral per unit mass of water). Semi-quantitative observations, however, are consistent with the overall evolution of the maturity of the sediment in the chronosequence. The regolith is almost entirely composed of primary rock-forming minerals from amphibolites, quartz-mica schists, marbles, carbonate schists, and phyllites (Czerny *et al.*, 1993). These rocks contribute mostly quartz and various feldspars, amphiboles, micas, chlorites, epidotes, as well as carbonates and sulphides as key components of the mineral framework of the regolith. The feldspars are usually Na-rich plagioclase. Carbonate minerals include calcite, dolomite, ankerite, and siderite (often Mn-rich siderite). The primary sulphides include pyrite, chalcopyrite, galena, and sphalerite. The analysis of the heavy fraction and the estimates presented by Szynkiewicz *et al.* (2013) indicate that sulphide minerals comprise up to 0.5 wt.% of mineral skeleton.

Primary clay minerals and iron (oxy)hydroxides are absent from the country rocks; their presence would indicate the formation of secondary weathering products. The products of weathering include goethite and several undetermined iron (oxy)hydroxides (identified using optical and electron microscopy) as well as secondary clay minerals (identified using XRD). In the X-ray diffraction patterns of random mounts (Fig. 4A), a *060* peak is apparent at ca. 1.49–1.50 Å, which reflects the presence of dioctahedral minerals. The reflections originated in the phyllosilicates chlorite and mica (muscovite, 2M1 politype on the basis of the peaks at 3.21, 2.99 and 2.87 Å) as well as quartz, feldspars and amphibole (probably hornblende) are apparent. A single, basal amphibole peak is clearly apparent only in the XRD patterns of samples C and M: it is barely detected in the pattern of sample F. The presence of biotite was evidenced by optical microscopy only. Also, since a *060* reflection of trioctahedral minerals at 1.54 Å coincides with the quartz *211* peak, their presence is not certain.

Clay minerals occur in the soils as well. In sample F, these are probably mica-smectite (M-S) and mica-vermiculite (M-V). This is evidenced by a weak and broad reflection, which occurs in the pattern of the air-dried sample at approximately 6–9 °2Θ (Fig. 4B). Ethylene glycol solvation results in a slight alteration of the peak shape, with a decrease in the peak intensity on the low-angle side. This feature indicates the presence of expandable layers. After heating at 550 °C, the peak disappears, which in turn indicates the presence of layers collapsing upon heating. The XRD pattern of the glycol-solvated M sample (Fig. 4B) shows a broad band at approximately 4.5–6 °2Θ, which disappears entirely after heating. This indicates the presence of smectite and/or disordered smectite–illite in the sample. XRD patterns of both the glycol-solvated and heated sample C reveal virtually no changes in the low 2Θ range (Fig. 4B), which evidences the absence of mixed-layered clays.

COMPOSITION OF THE PORE WATER

The physicochemical parameters of pore waters are presented in Table 4. The systematic changes between samples correlate with distance from the glacier front: pH decreases from 8.57 to 7.72 and TDS increases from 123 to 748 mg/L, while Eh decreases from 270 to 174 mV. Similar changes in major ion concentrations are also apparent (Fig. 5). The chloride content increases toward the coast from 8 to 21 mg/L. Ocean water aerosol present in the atmospheric precipitation is probably the major source of Cl^-. Aerosol is also partially responsible for the input of Na^+, K^+, Mg^{2+} and SO_4^{2-}. By comparison with the products of weathering, however, the input of these ions from aerosol (estimated on the basis of Cl^- concentration and the proportion of ions in the sea water) is insignificant.

The concentration of HCO_3^- increases with distance from the glacier as well (Fig. 5). However, the relative content, expressed as the percentage of bicarbonate in TDS, decreases from 53% in the C sample, through 40% in the M sample, to 32% in the F sample. In contrast to HCO_3^-, the percentage of SO_4^{2-} in TDS increases down the chronosequence from 12% through 33% to 40%. Hence, the waters evolve from carbonate-dominated to sulphate-dominated.

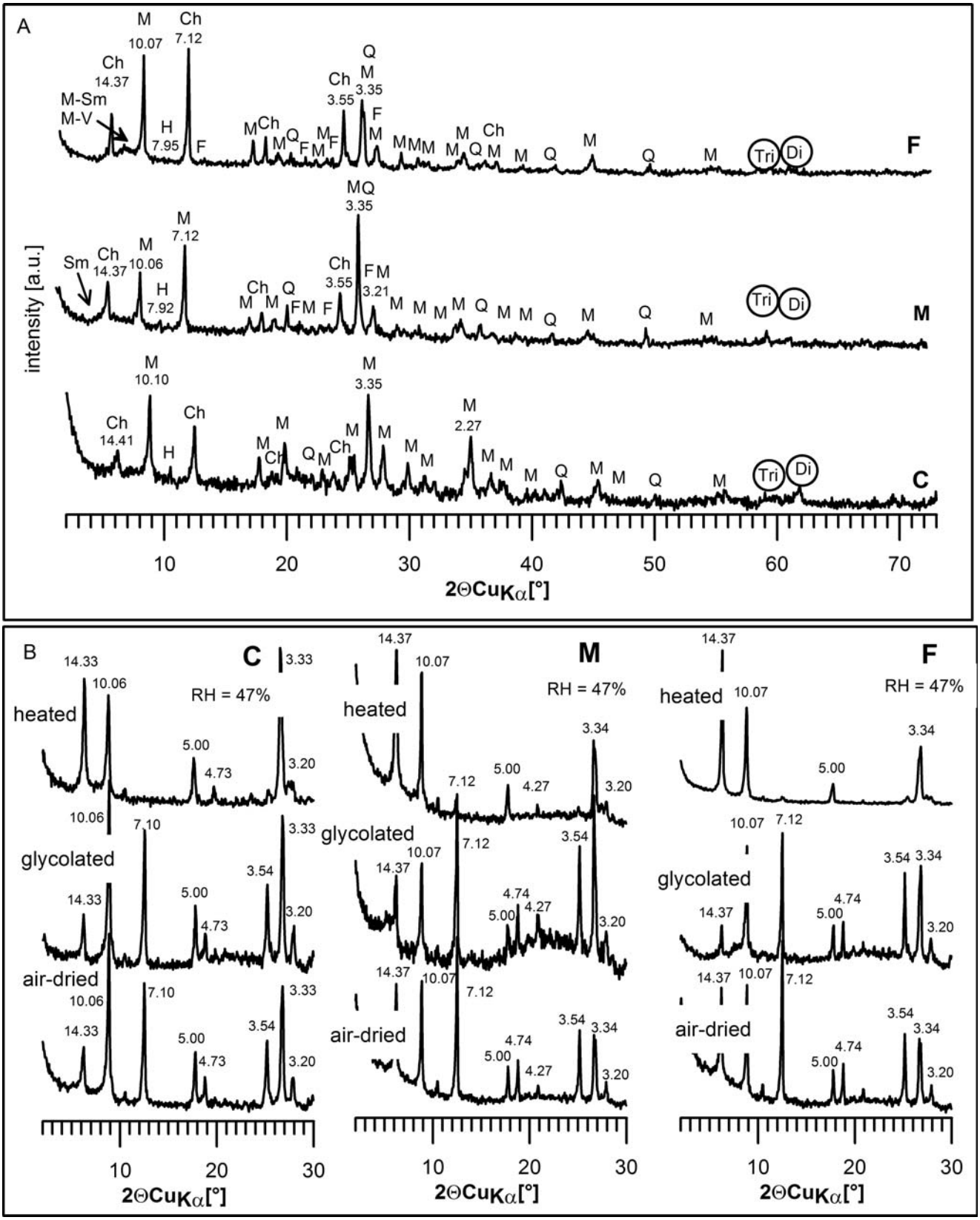

Fig. 4. X-ray diffraction patterns of the clay (< 2 μm) fractions. **A.** Unoriented specimens. **B.** Air-dried, glycol-solvated and 560 °C-heated samples. Explanations: Ch – chlorite, M – muscovite, H – hornblende, Q – quartz, F – feldspar, M-Sm mica-smectite, M-V – mica-vermiculite, Sm – smectite and/or smectite-illite, Di – *060* peak of dioctahedral minerals, Tri – *060* peak of trioctahedral minerals, RH – relative humidity.

Table 4

Chemical composition of waters; concentration of ions in mg/L

	Glacial runoff	C 20 m	M 950 m	F 1700 m
Ca^{2+}	8.67	20.8	91.2	131.2
Mg^{2+}	b.d.	8.65	39.95	45.1
Na^{+}	0.95	0.46	5.51	6.34
K^{+}	0.8	2.53	4.46	4.78
Li^{+}	n.a.	0.0003	0.0003	0.0036
Fe^{2+}	n.a.	0.032	0.086	0.119
Mn^{2+}	0.013	0.001	0.019	0.032
Sr^{2+}	n.a.	0.0310	0.161	0.251
Ba^{2+}	n.a.	0.0157	0.021	0.016
Al^{3+}	n.a.	0.0112	0.002	0.0017
NH_4^{+}	0.048	0.032	0.026	0.031
HCO_3^{-}	13.6	64.8	226.8	236.52
SO_4^{2-}	0.23	15	188	300
Cl^{-}	12	8.5	14.2	21.3
NO_3^{-}	n.a.	0.48	0.406	0.242
F^{-}	n.a.	b.d.	0.389	0.427
Ion balance	1.30	6.29	0.87	–0.38
SiO_2	0.117	1.732	1.720	2.045
pH	8.97	8.57	7.75	7.72
Eh [mV]	244.7	270.4	330.4	174.7
EC [µS/cm]	37.11	140	630	746
O_2 mg/L	13.42	10.58	5.16	9.51
TDS mg/L	36.63	123.07	572.95	748.41
Type of water		Ca-Mg-HCO_3	Ca-Mg-SO_4-HCO_3	Ca-SO_4

b.d. – below detection, n.a. – not analyzed

The evolution of the waters is dominated by changes in the concentration of Ca^{2+}, SO_4^{2-}, HCO_3^{-}, and Mg^{2+} (Fig. 6). The evolution of bicarbonate correlates with that of magnesium, which may indicate that for the most part both result

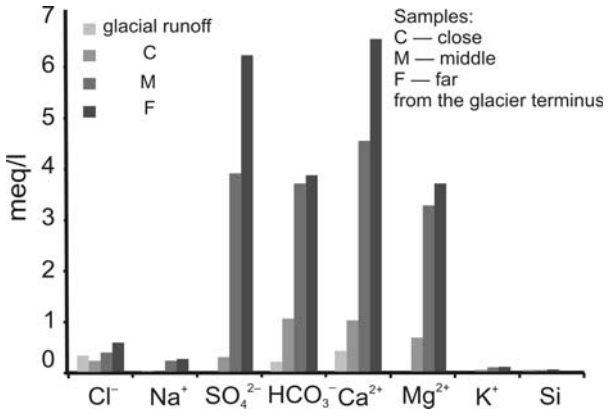

Fig. 5. Concentration of ions in pore waters; the increase down the chronosequence is apparent.

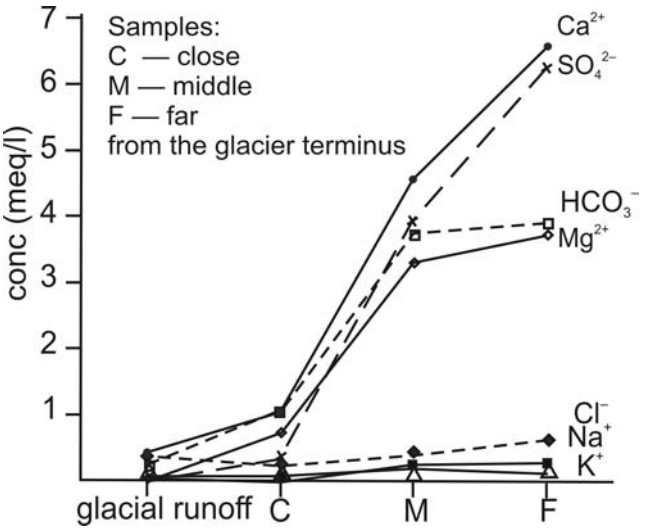

Fig. 6. The evolution of pore water composition. The pattern indicates the dominating effect of equilibrium with carbonate and sulphate minerals.

from the dissolution of carbonates. Calcium strongly correlates with sulphate indicating the importance of equilibrium with gypsum. The significant proportion of Ca^{2+} and SO_4^{2-} ions present in the solutions may have resulted from the dissolution of secondary sulphate salts, formed by freeze-driven concentration in winter. Such formation of secondary sulphates on the surface of the moraine was observed, not only in the foreland of Werenskioldbreen, but also near Finsterwalderbreen (Wadham *et al.*, 2007; Szynkiewicz *et al.*, 2013).

DISCUSSION OF OBSERVED WEATHERING FEATURES

Weathering features observed on the surface of rock-forming minerals separated from the sediments studied allow identification of the major reaction mechanisms (Fig. 7). It is significant that the morphology of etch pits and the formation of secondary phases apparent on mineral surfaces were identical, regardless of the distance from the glacier terminus. This might indicate that the apparent mechanisms of the processes are the same and do not change at least within ca. 70 years of exposure.

The dissolution of carbonate minerals is a major source of Ca, Mg, Fe and bicarbonate ions in the solutions. SEM imaging indicates that the dissolution of carbonate minerals begins along crystallographic directions, such as the oriented etch pits, formed on the surface of a calcite grain (Fig. 7A). Deeply etched cleavage is apparent and triangular etch pits show a crystallographic orientation (Fig. 7A–C). The secondary products of weathering were precipitated inside the etch pits. The dissolution of carbonate minerals containing Fe was accompanied by Fe oxidation, resulting in the precipitation of iron oxyhydroxides (e.g., goethite FeOOH). The dissolution of carbonate minerals, mostly calcite, is advanced by comparison with other minerals. This observa-

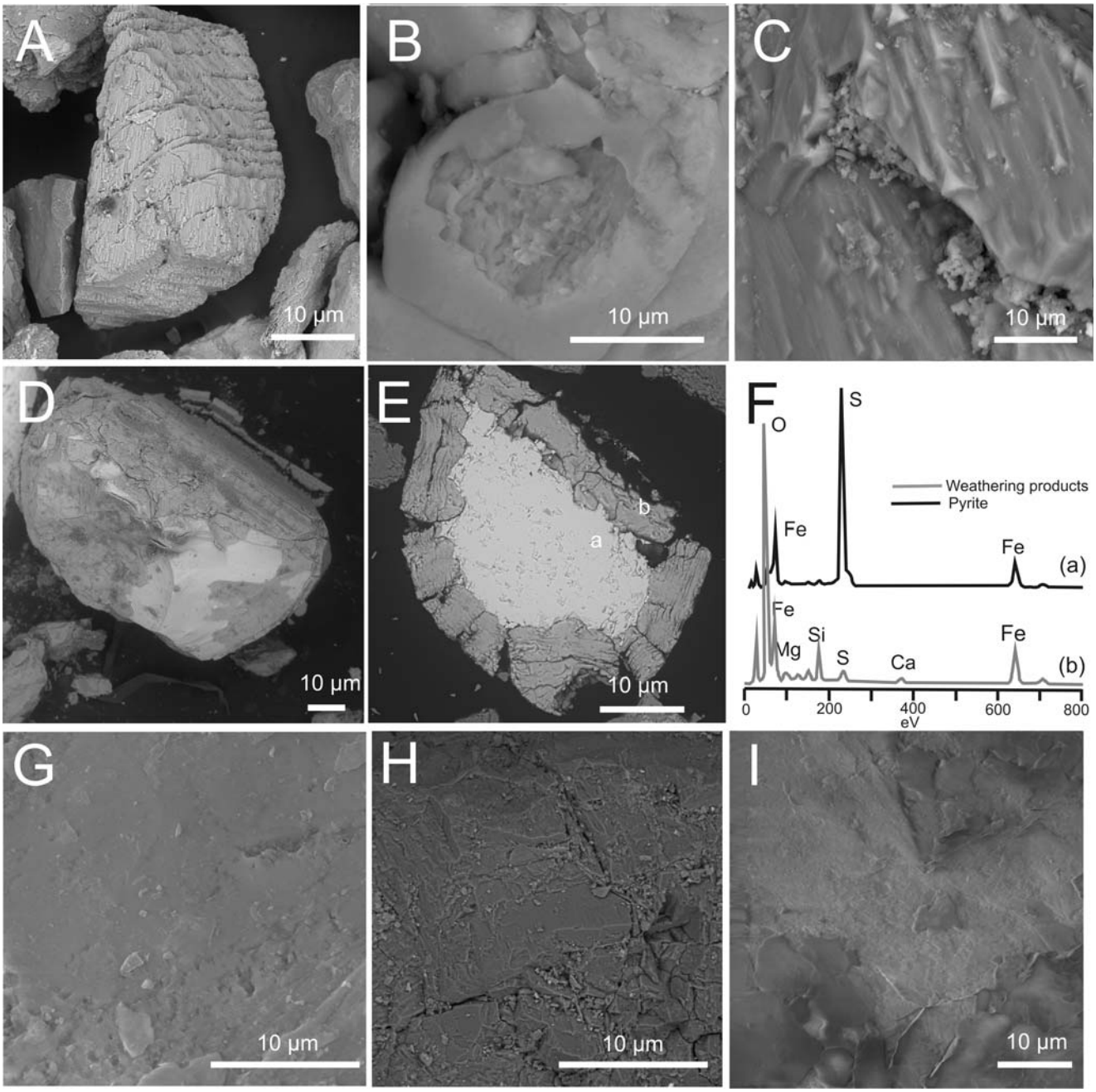

Fig. 7. The morphology of etch pits and the formation of secondary phases on selected mineral grains. All samples are from M (middle) sampling site. SEM images, scale bars – 10 µm. **A–C.** Deeply etched cleavage, crystallographically oriented, triangular etch pits and secondary Fe (oxy)hydroxides on the surface of calcite (A, B) and Fe-bearing dolomite (C). **D–F.** Surface (D) and cross- section (E) of weathered pyrite with EDS spectrum (F) of elemental composition at spots marked, indicating formation of oxidized crust. **G–I.** Surface of weakly weathered amphibole, biotite and plagioclase, respectively.

tion is consistent with the path of weathering described previously for the Werenskioldbreen and similar polythermal glaciers in Spitsbergen (Wadham *et al.*, 1997, 2001, 2007; Hodson *et al.*, 2000; Cooper *et al.*, 2002, 2011; Bukowska-Jania, 2007; Szynkiewicz *et al.*, 2013).

The unaltered cores of pyrite grains are always covered with layers of easily exfoliating weathering products, mostly goethite (Fig. 7D, E). Iron oxyhydroxides were identified with an optical microscope (reflected light) and by chemical analysis using SEM-EDS: the spectrum of the fresh surface of pyrite indicates the presence of iron and sulphur, while the altered surface layers consist of Fe and O, plus some Mg, Ca, S and Al (Fig. 7F). This evidence supports the choice of the reactions used in the computer simulations. Pyrite is considered here as an example, illustrating the processes associated with oxidation of all sulphides in the moraine. The weathering of pyrite and other sulphides was responsible for the presence of SO_4^{2-} ion in the pore waters. The role of anoxic oxidation reported from the foreland of the similar Finsterwalderbreen, located ca. 50 km north, is

unclear here (Wadham *et al.*, 2007). Anoxia was probably less common in the surface layer of soil during sampling in July, when the active layer was much deeper than the sample depth equal to 30 cm. The SO_4^{2-} content in the water increases with distance from the glacier front, i.e. with the age of soil and the advancement of the weathering of sulphide minerals.

Dissolution etch pits were observed also on the surfaces of all amphiboles (Fig. 7G). The crystallographic orientation and geometrical shape of the etch pits indicate a surface-controlled mechanism of dissolution. At the initial stages of amphibole weathering, Ca and Mg are released preferentially for structural reasons (Wilson, 2004) and then the dissolution becomes congruent and linear. Further weathering may result in the formation of secondary phases, such as hydrous phyllosilicates, iron oxyhydroxides (e.g., ferrihydrite and/or goethite) and anatase (Churchman, 2000). However, secondary phases were not apparent on the grains examined. This indicates that the amphibole is at a very early stage of weathering. Yet, since examination of limited number of grains by SEM does not provide fully representative information, the formation of phyllosilicates or iron oxyhydroxides resulting from amphibole weathering cannot be ruled out completely.

The sharp edges on the surface and the dissolution features of Na-rich plagioclase are parallel to the cleavage (Fig. 7I). In addition to weathering progressing at the edges and etch pits, exfoliating layers are also apparent. Unidentified secondary phases were observed on plagioclase grains, separated from all three soil samples. According to Wilson (2004), dislocations, defects, and micro-textural features play the most significant role in the dissolution of the exposed surface of plagioclase.

Chemical transformation of micas and chlorites were observed with both optical and electron microscopy (Fig. 7H). Dissolving biotite and amphiboles are potentially the most important sources of K. Biotite is much more susceptible to weathering than muscovite. It may be transformed to vermiculite or kaolinite (Wilson, 2004). Chlorite may be progressively converted to vermiculite (and ultimately to kaolinite or halloysite) and fine-crystalline Fe oxyhydroxides (Murakami *et al.*, 1996). However, direct evidence of biotite or chlorite transformation in the soils from the Werenskioldbreen moraine is limited.

Secondary clay formation by weathering in the foreland of retreating glacier in polar conditions is a broad issue, beyond the scope of this paper. Sampling and mineral analysis procedures for the purpose of geochemical modelling are not systematic enough for the detailed analysis of clays, which require a specific approach. The presence of mixed-layered clays (mica-vermiculite, smectite-illite) was detected with XRD mostly in sample F, which was undergoing weathering for at least 70 years. However, direct mechanisms of formation were not identified for them.

The increase in total mineralization of pore waters in the chronosequence might represent the role of advancement of weathering from initial stages at C to more matured stages at F. The sediments in the foreland of the Werenskioldbreen are very rich in carbonate minerals. This feature and the short time span of the chronosequence are probably the reasons why the three samples represent snapshots of the system in its early stages, gradually approaching equilibrium. With time, when easily weathering minerals become exhausted and equilibrium is governed by aluminosilicates, the mineralization of solutes probably declines. This was observed in the foreland of the Bench Glacier in Alaska (Anderson *et al.*, 2000). This might also indicate that pore waters, soaking and slowly percolating through these poorly sorted sediments, have more time to react with the mineral framework than running surface waters, which were analyzed in the foreland of the Bench Glacier.

Saturation indices (SI) were calculated for calcite and gypsum using the PHREEQC speciation code (Parkhurst, 1995). It is defined as the logarithm of the ratio of ion activity product (IAP, based on the concentrations measured) to the theoretical solubility product (K_{sp} from tables). This way, SI calculated for each mineral can be negative for an undersaturated solution, positive for an oversaturated solution, and equals zero for a solution in equilibrium with respect to the mineral under consideration. The saturation indices of calcite and gypsum increase systematically from glacial runoff through waters C, M to F. The SI for calcite equal –0.5, 0.1, 0.3, and 0.4 in the glacial runoff and at sites C, M and F, respectively. This is close to zero (within a precision equal to ± 1.0), indicating a saturation state close to equilibrium. The SI for gypsum shows undersaturation and increases from –4.8 in glacial runoff to –2.7, –1.3, and –1.0 in C, M and F, respectively. This might indicate that pore waters in more matured soil quickly reach equilibrium with carbonate minerals, while being continuously supplied with SO_4^{2-} from the oxidation of sulphides. The soils are an open system, so that slowly percolating rain and melt waters result in continuous mineral dissolution. The weathering of carbonates advances faster than the weathering of sulphides. Therefore, the dissolution of carbonate minerals (mainly calcite, dolomite, ankerite and siderite) is a dominant weathering process in the newly exposed sediments. This explains the dominance of HCO_3^-, Ca^{2+} and Mg^{2+} in the soil pore water. Some Ca^{2+} and Mg^{2+} result from the weathering of rock-forming aluminosilicates as well (e.g., biotite and other black micas, amphiboles, chlorites, plagioclases etc.). The oxidation of pyrite and other sulphides is a major source of SO_4^{2-}. The progress of sulphide weathering is slower than that of carbonates and becomes a significant part of the system in more matured soils, far from the glacier terminus. Sulphide oxidation is coupled to carbonate dissolution:

$$4FeS_{2(s)} + 16CaCO_{3(s)} + 15O_{2(g)} + 10H_2O = 16Ca^{2+} + 16HCO_3^- + 8SO_4^{2-} + 4FeOOH_{(s)}$$

This reaction is responsible for the pattern of increasing partial pressure P_{CO_2} and increasing dominance of SO_4^{2-} ions over other aqueous constituents in the path from glacial runoff to pore waters far from the glacier. On the basis of P_{CO2} calculated using PHREEQC, glacial runoff waters are undersaturated with respect to CO_2 ($P_{CO_2} = 10^{-4.94}$ atm), the pore water at locality C is close to saturation ($P_{CO2} = 10^{-3.86}$ atm), and pore water at localities M and F are oversaturated with respect to CO_2 ($P_{CO_2} = 10^{-2.51}$ atm and $10^{-2.47}$ atm, respectively). In the reaction above, the oxidation of sulphides supplies protons for the weathering of car-

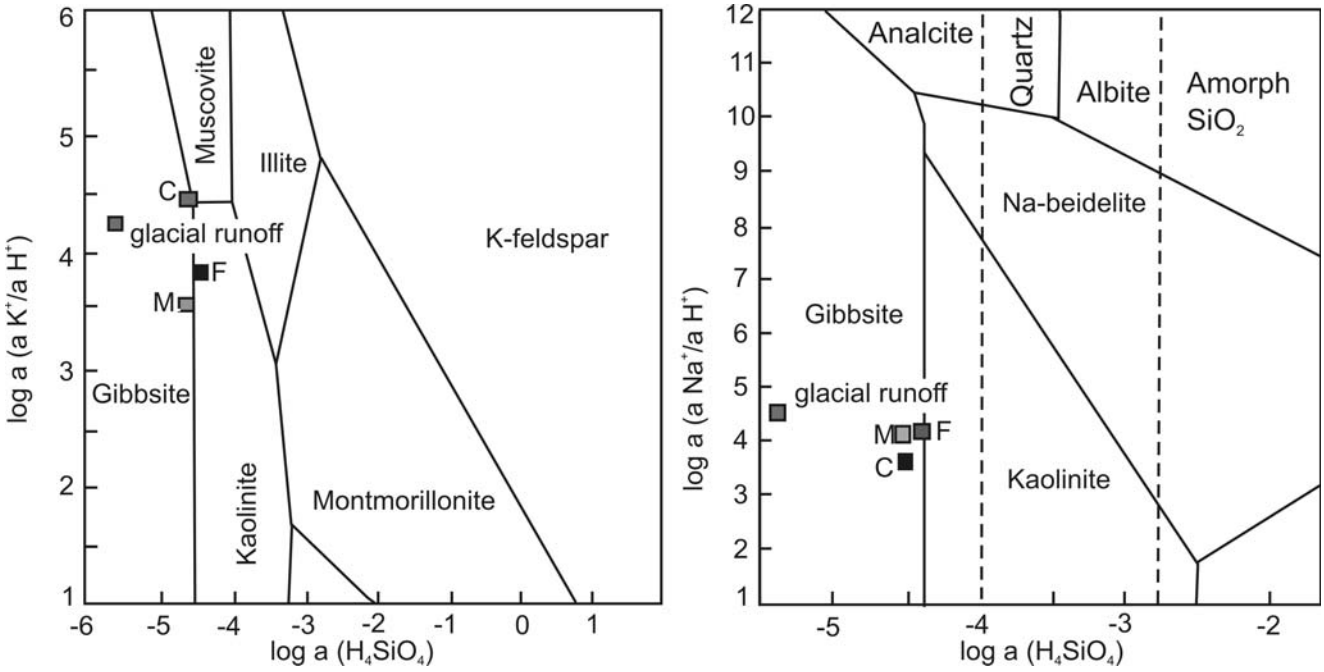

Fig. 8. Mineral stability diagrams with the position of samples projected. Left: system K_2O – Al_2O_3 – SiO_2 – H_2O, right: system Na_2O – Al_2O_3 – SiO_2 – H_2O (after Lecomte *et al.*, 2005). All three pore water analyses plot at the border between gibbsite and kaolinite, indicating that these are potentially the most stable secondary phases in these systems.

bonates, which generates P_{CO_2} exceeding that in the atmosphere. Thus, the chemical weathering processes of sediments containing carbonates in the foreland of retreating glaciers are a source, rather than a sink, of CO_2 to the atmosphere (Wadham *et al.*, 2001, 2007; Cooper *et al.*, 2002).

THERMODYNAMIC MODELLING

The reactions considered in the mass balance calculations represent a limited number of dissolution/precipitation and oxidation/reduction processes which is obviously a simplification of the system. However, these are the types of reaction, which allow explanation of the evolution of pore water composition. Several assumptions have been made in this model. It is assumed that the composition of the pore water is derived from the glacial melt and atmospheric precipitation. The chloride comes from sea salt. All other chemical constituents result from mineral-water interaction. The input of other ions from aerosol, based on Cl^- concentration and the proportion of ions in sea water, is negligible compared to the measured solute concentration. The dissolution of calcite, dolomite and siderite represent reactions with carbonate minerals. Manganese-rich siderite $Fe_{0.7}Mn_{0.3}CO_3$ is used in the model on the basis of the SEM-EDS analyses of siderite grains separated from the sediments. The primary aluminosilicates include albite, plagioclase, biotite, and hornblende. Pyrite is the only primary sulphide and represents a major phase contributing to the redox processes. Incongruent dissolution of aluminosilicates and pyrite is demonstrated by precipitation of the secondary phases goethite, vermiculite, illite, kaolinite, and smectite. All the assumed possible reactions and phases included in the simulations are justified, either by direct observations supported by the evidence from the literature or by the activity diagrams. The dissolution of carbonate minerals is indicated by the pH of pore waters, their saturation with respect to carbonate minerals, the etch pits observed on the surfaces of mineral grains, and by the detailed study of Bukowska-Jania (2007). Goethite rims observed around pyrite grains support the oxidation reaction of Fe sulphide. A sodium content of 62 mol. % Na in the plagioclase was confirmed by direct elemental analysis using SEM-EDS. Kaolinite was encountered as a weathering product of feldspar and mica in the clay fraction of glacial moraines in crystalline rock terrains (Alexander and Burt, 1996). Additionally, stability diagrams were used to narrow the list of potential secondary clay minerals. The PHREEQC speciation calculation was used to obtain the activity of Na^+, K^+, H^+, and H_4SiO_4. These values were then projected on the mineral stability diagrams, presented in Fig. 8. Two stability diagrams were used: the Na_2O – Al_2O_3 – SiO_2 – H_2O system and the K_2O – Al_2O_3 – SiO_2 – H_2O system (Lecomte *et al.*, 2005). All three pore water analyses plot at the border between gibbsite and kaolinite, indicating that these are the most stable phases. Kaolinite and gibbsite were not detected in the mineral framework of the regolith samples under consideration within the detection limits of X-ray diffraction equal to ca. 1 wt.%. Both minerals, however, were included in the inverse modelling input file as thermodynamically possible secondary phases accommodating the excess of Al and Si.

The objective of inverse geochemical modelling was to identify specific dissolution and precipitation reactions, consistent with the observed mineral alterations responsible for the evolution of water composition observed. In inverse modelling, the computer code PHREEQC calculates the

Table 5

Results of inverse modeling using PHREEQC presented in percentage of moles of minerals dissolved (upper part) and precipitated (lower part) indicating relative participation in weathering; four thermodynamically plausible scenarios have been chosen for sample C and six for M and F; grey – the models which are in closest agreement with the observed mineral transformation reactions

Sample	C				M						F					
	Alternative models				Alternative models						Alternative models					
	1	2	3	4	1	2	3	4	5	6	1	2	3	4	5	6
Percent of phases dissolved																
Calcite	18	19	19	18	15	15	13	13	8	8	36	36	38	38	36	36
Dolomite					34	34	39	39	46	46	19	22	19	19	22	19
Siderite	59	61	61	59	18	18	11	11	6	6	<1	<1	<1	<1	<1	<1
K-feldspar	4			4					3	3	2					2
Plagioclase					4	4	8	8	9	9	7	4	7	7	4	7
Biotite		4	4				2	2								
Pyrite	7	7	7	7	27	27	27	27	28	28	30	33	31	31	33	30
Chlorite	11	9	9	11							5	3	4	4	3	5
Hornblende					2	2						2			2	
Percent of phases precipitated																
Kaolinite	11		9			11		11		13		14		15		16
Gibbsite		15		17	16		17		19		22		21		20	
Chalcedony	14	24	13	27	31	19	35	24	38	27	39	23	38	24	36	25
Pyrolusite	15	12	16	11	6	8	4	5	2	3	<1	<1	<1	<1	<1	<1
Goethite	60	49	62	45	47	62	44	60	41	57	39	63	42	60	44	59

possible amounts of moles of mineral phases involved in the transformation reactions in agreement with observed mass balanced evolution of pore water composition, which was determined analytically. The input data include the chemical composition of the initial and final solutions, and the minerals involved in the reactions. Alternative sets of thermodynamically plausible mineral-water interaction reactions were calculated to explain the evolution of water composition on the basis of specific assumptions. This way, the key players of the system can be identified and the semi-quantitative weight of their role can be estimated. The results provide a thermodynamic rationale for linking the microscopically observed mineral transformations with the macroscopic values of pore water composition. Comparison of the results between the sites represents the evolution of the dominating transformation processes in the chronosequence in time and space.

Computer simulations were performed separately for each locality for a pathway from glacial runoff towards pore water. Glacial runoff was chosen as a proxy for the initial composition of the solution. There was no technical possibility to collect snow or rain water during the time of sampling the pore waters. The choice of rain or snow composition from the literature seems to be too simplistic. The observation of the surface of the Werenskioldbreen foreland for many years in different seasons by the present authors indicates that the composition of pore water is derived from the mixing of glacial melt, snow melt and atmospheric precipitation at different times of melting in the spring and summer. Therefore, the average composition of water entering the system has a higher mineralization than pure rain and snowmelt. This mineralization results from reactions with rocks present in the area. It is assumed here that the stream water sampled very close to the glacier terminus approximates the maximum mineralization of the initial solution coming from the glacier and entering the regolith. In reverse modelling, the sampled pore water composition was used as the initial solution, while glacial runoff, approximated by the composition of a creek, was used as the target solution. The model input files consisted of field-measured pH, temperature, and the concentration of ions and SiO_2. Water chemistries were used as determined without adjustments. The ion balance errors were between –0.38% and 6.29%. Metal concentrations below the detection limit were not used in the input files.

The inverse modelling generated several possible scenarios to explain the evolution of the pore water chemistry determined in the field (Table 5). Out of 14 models resulting from modelling with the use of the pore water composition from locality C (closest to the glacier), four were chosen as plausible scenarios. Only models which included calcite were selected. Siderite, pyrite, and chlorite dissolution is included in all of these models. The dissolution of biotite or K-feldspar is a source of potassium. The formation of secondary pyrolusite, goethite, and chalcedony is predicted. The precipitation of gibbsite (or kaolinite) serves as an alternative sink of aluminum. The redox reaction includes the oxidation of Fe^{2+} and S^{2-} and reduction of oxygen. It is sig-

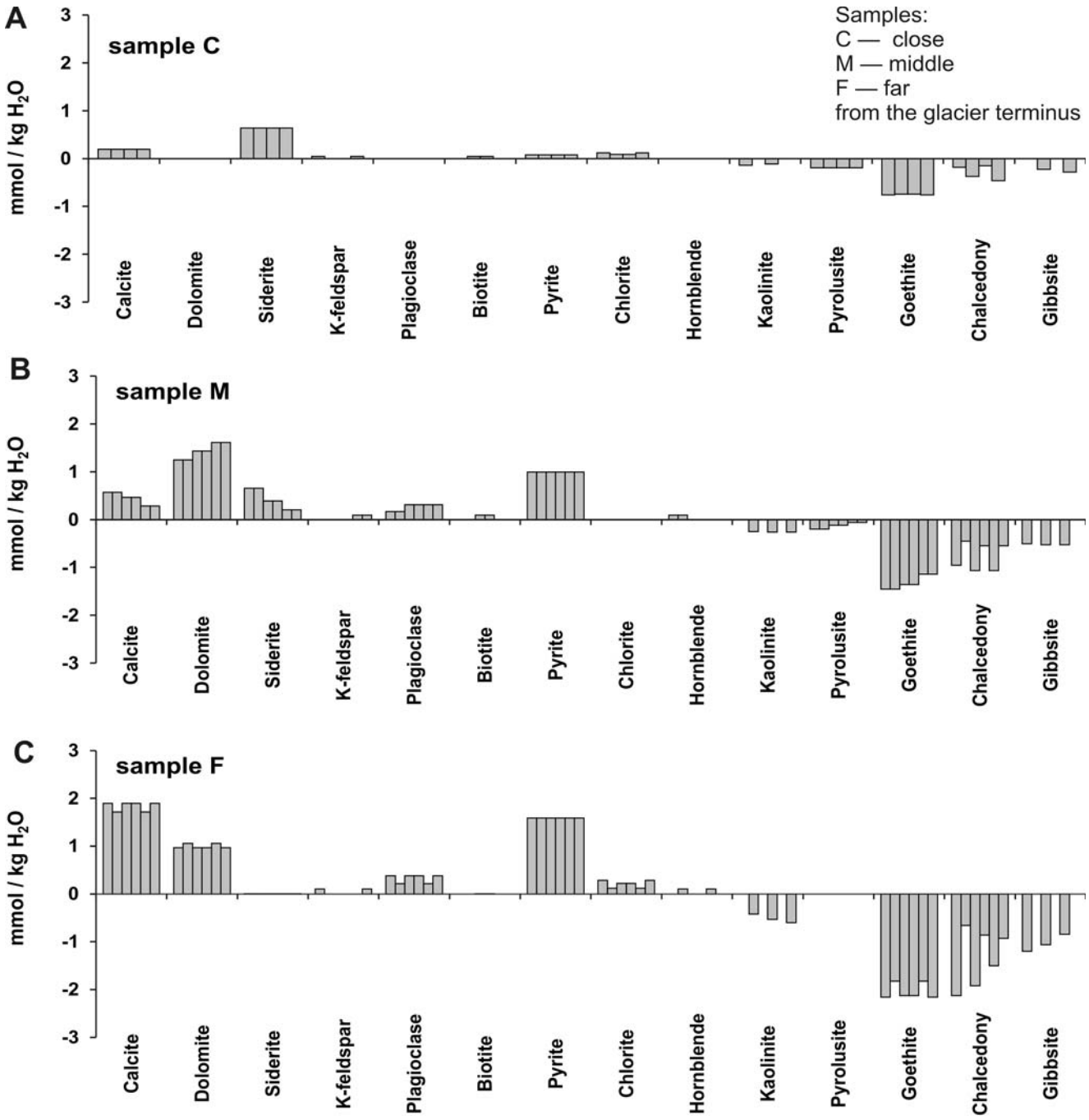

Fig. 9. Comparison of mass balance calculations by PHREEQC (expressed as mole transfers per kilogram of water), indicating the increase in contribution of dissolution (positive values) and precipitation (negative values) reactions to pore water composition in a chronosequence. Each bar distinguished in gray scale represents a separate (alternative) model: four models for C and six for M and F. The bars oriented upwards indicate dissolution, while the bars pointing downwards indicate precipitating phases. **A.** Sample C. **B.** Sample M. **C.** Sample F.

nificant that dolomite, plagioclase and hornblende are not included in the list of minerals reacting with the solution. This indicates that, present or not, these minerals do not contribute to the evolution of the composition of the solution. It seems that the presence of more soluble minerals in the system is sufficient to explain the evolution of the water. However, the lack of dolomite in the model and the presence of chlorite as the sole source of Mg are quite unrealistic. The removal of chlorite from the list of minerals results in even less realistic models, which ignore the dissolution of calcite. These are the limitations of the model.

For the pore waters sampled at locality M, 12 models resulted from inverse modelling. Only 6 models, which included the dissolution of dolomite in the reaction path, were selected for further discussion. All models include also the dissolution of calcite, siderite, and plagioclase, along with the precipitation of pyrite, goethite and chalcedony. The dissolution of hornblende, biotite, or K-feldspar is a source of K.

The dissolution of dolomite is a source of Mg. The precipitation of gibbsite (or kaolinite) is an alternative sink for Al.

The inverse modelling of pore water from locality F (far from the glacial front) also resulted in 12 models, out of which 6 were selected. The results presented in Table 5 in terms of percentages indicate that far from the glacier terminus the system is still dominated by the dissolution of carbonate minerals (over 50% of released moles of solutes), but the contribution resulting from the weathering of pyrite becomes significant (over 30%). The dissolution of plagioclase and chlorite is a source of Al and Si, complemented with K-feldspar, biotite and hornblende, alternatively serving as sources of K. As in other models, gibbsite or kaolinite are the alternative sinks for Al.

The differences between the models within the samples are practically insignificant. The list of plausible scenarios is narrowed down to a few alternative solutions (Table 5). For example, models C1 and C4 differ from models C2 and C3 in the source of K being the dissolution of K-feldspar or biotite. They also differ in the reaction products being gibbsite (models 1C and 3C) or kaolinite (models 2C and 4C). The presence of chlorite depends on the presence of dolomite, since these are the only sources of Mg. This is one of the limitations of thermodynamic modelling. Similarly, equivalent solutions result from the simulations of water evolution for sample M and F. The models, which are in closest agreement with the mineral transformation reactions observed, are marked in grey in Table 5. The numbers show the percent contribution of each mineral to the evolution of water chemistry observed.

The comparison of the results between sampling sites, normalized to moles transferred (moles of minerals dissolved or precipitated) per kilogram of water, allows the use of semi-quantitative observations (Fig. 9). The amount of dissolution, indicated by the size of the bars oriented upwards, increases from location C to location F. This contributes to the solutes in pore waters, resulting in the observed increase of TDS. The total amount of dissolved carbonate minerals responsible for the mineralization of waters decreases from C through M to F, while the amount of dissolved/oxidized pyrite increases. This provides thermodynamic confirmation of the fact that the relative significance of carbonate weathering decreases and that of sulphide increases down the chronosequence. The participation of silicate minerals in weathering remains roughly the same: with the dissolution of aluminosilicates, followed by the precipitation of secondary gibbsite (or kaolinite), probably more significant in the oldest soil system. This thermodynamic modelling does not include the kinetics of the reactions or microbially mediated processes.

CONCLUSIONS

It is significant that the morphology of etch pits and the formation of secondary phases on mineral surfaces were identical, regardless of the distance from the glacier terminus. This might indicate that the mechanisms of particular weathering processes are the same at the initial as well as at more mature stages and do not change at least within ca. 70 years of exposure. The crystallographic orientation and geometrical shape of the etch pits indicate a surface-controlled, rather than a diffusion-controlled mechanism of dissolution. This means that the weathering rate depends strongly on the kinetics of particular mineral transformations, rather than on pore water movement and percolation. Therefore, microbial processes affecting directly the mineral-water interface may play a significant role in this system.

Tranter *et al.* (2002), on the basis of the composition of waters sampled from boreholes, found indirect evidence for the advanced weathering of carbonates, silicates, and sulphides underneath an Alpine glacier. In contrast, the pore waters and recently uncovered sediments in the forefield of Werenskioldbreen represent a very immature system. The processes speed up rapidly upon exposure and the maturity increases quickly with distance from the glacier. This is probably not only a result of exposure to the atmosphere and seasonal changes, but most certainly an effect of the enhancement of microbial activity as well, which is an objective of ongoing research.

As was observed at the foreland of Finsterwalderbreen (Spitsbergen), the chemical weathering processes of sediments containing carbonates in the foreland of the retreating glacier are a source, rather than a sink of CO_2 to the atmosphere. Despite ca. 70 years of exposure, this system is still in the initial stages of weathering and is dominated by processes involving carbonates, sulphates and sulphides. The relative contribution from sulphides, estimated with semi-quantitative thermodynamic modelling, increases down the chronosequence. The contribution from silicate minerals in the interaction between the framework of grains and pore waters is small but may become more significant after carbonate and sulphide sources have been exhausted. This stage has not yet been reached in the chronosequence under consideration because the sediments are relatively rich in carbonate and sulphide minerals. This might prevent a straightforward comparison of this young chronosequence with the usually older Alpine sites.

Acknowledgements

We would like to thank Jerzy Czerny for the help in the field and Adam Gaweł for assistance in the interpretation of the XRD patterns. Furthermore, the authors are indebted to Suzanne P. Anderson, Michał Skiba, Marek Matyjasik, and an anonymous reviewer for their helpful comments and suggestions, which improved the manuscript to a large extent. This work was supported by NCN Grant N N307 473638. A.M.P. acknowledges funding from AGH Research Grant No 11.11.140.319.

REFERENCES

Alexander, E. B. & Burt, R., 1996. Soil development on moraines of Mendenhall Glacier, southeast Alaska. 1. The moraines and soil morphology. *Geoderma*, 72: 1–17.

Anderson, S. P., 2007. Biogeochemistry of glacial landscape systems. *Annual Review of Earth and Planetary Sciences*, 35: 375–399.

Anderson, S. P., Drever, J. I., Frost, S. D. & Holden, P., 2000. Chemical weathering in the foreland of a retreating glacier.

Geochimica et Cosmochimica Acta, 64: 1173–1189.

Anderson, S. P., Drever, J. I. & Humphrey, N. F., 1997. Chemical weathering in glacial environments. *Geology*, 25: 399–402.

Bernasconi, S. M. & BigLink Project Members, 2008. Weathering, soil formation and initial ecosystem evolution on a glacier forefield: a case study from the Damma Glacier, Switzerland. *Mineralogical Magazine*, 72: 19–22.

Bradley, J. A., Singarayer, J. S. & Anesio, A. M., 2014. Microbial community dynamics in the forefield of glaciers. *Proceedings of the Royal Society B*, 281: 1–8.

Brantley, S. L., 2003. Reaction kinetics of primary rock-forming minerals under ambient conditions. *Treatise on Geochemistry*, 5: 73–117.

Bukowska-Jania, E., 2003. *The Role of Glacier Systems in the Migration of Calcium Carbonate in the Natural Environment.* Katowice, Wydawnictwo Uniwersytetu Śląskiego, 248 pp. [In Polish, with English summary.]

Bukowska-Jania, E., 2007. The role of glacier system in migration of calcium carbonate on Svalbard. *Polish Polar Research,* 28: 137–155.

Bukowska-Jania, E. & Jania, J., 1988. Changes in geometry of front of Werenskiold Glacier (Spitsbergen) in 1957–1983. In: *Wyprawy Polarne Uniwersytetu Śląskiego 1980–84*. Prace Naukowe Uniwersytetu Śląskiego nr 910. Wydawnictwo Uniwersytetu Śląskiego, Katowice, pp. 65–91. [In Polish.]

Churchman, G. J., 2000. The alteration and formation of soil minerals by weathering. In: Summer, M. E. (ed.), *Handbook of Soil Science*. CRC Press, Boca Raton, pp. F-3–76.

Cooper, R., Hodgkins, R., Wadham, J. & Tranter, M., 2011. The hydrology of the proglacial zone of a high-Arctic glacier (Finsterwalderbreen, Svalbard): Sub-surface water fluxes and complete water budget. *Journal of Hydrology*, 406: 88–96.

Cooper, R. J., Wadham, J. L., Tranter, M. & Peters, N., 2002. Groundwater hydrochemistry in the active layer of the proglacial zone, Finsterwalderbreen, Svalbard. *Journal of Hydrology,* 296: 208–223.

Czerny, J., Kieres, A., Manecki, M. & Rajchel, J., 1993. *Geological Map of the SW part of Wedel Jarlsberg Land Spitsbergen, 1:25 000*. Edited by Manecki, A. Institute of Geology and Mineral Deposits, University of Mining and Metallurgy, Krakow.

Czerny, J., Lipień, G., Manecki, A. & Piestrzyński, A., 1992a. Geology and ore mineralization of Hecla Hoek Succession (Precambrian) in front of Werenskioldbreen, South Spitsbergen. *Studia Geologica Polonica*, 48: 68–114.

Czerny, J., Pływacz, I. & Szubała, L., 1992b. Siderite mineralization in the Hecla Hoek Succession (Precambrian) at Strypegga, South Spitsbergen. *Studia Geologica Polonica*, 48: 154–170.

Dahms, D., Favilli, F., Krebs, R. & Egli, M., 2012. Soil weathering and accumulation rates of oxalate-extractable phases derived from alpine chronosequences of up to 1 Ma in age. *Geomorphology*, 151–152: 99–113.

Dümig, A., Smittenberg, R. & Kögel-Knabner, I., 2011. Concurrent evolution of organic and mineral components during initial soil development after retreat of the Damma glacier, Switzerland. *Geoderma*, 163: 83–94.

Hodgkins, R., Cooper, R., Wadham, J. & Tranter, M., 2009. The hydrology of the proglacial zone of a high-Arctic glacier (Finsterwalderbreen, Svalbard): Atmospheric and surface water fluxes. *Journal of Hydrology*, 378: 150–160.

Hodson, A., Tranter, M. & Vatne, G., 2000. Contemporary rates of chemical denudation and atmospheric CO_2 sequestration in glacier basins: an Arctic perspective. *Earth Surface Processes and Landforms*, 25: 1447–1471.

Huggett, R. J., 1998. Soil chronosequences, soil development, and soil evolution: a critical review. *Catena*, 32: 155–172.

Jania, J. & Hagen, J. O. (eds), 1996. *Mass Balance of Arctic Glaciers.* IASC Report No. 5. University of Silesia, Sosnowiec – Oslo. 62 pp.

Kabała, C. & Zapart, J., 2009. Recent, relic and buried soils in the forefield of Werenskiold Glacier, SW Spitsbergen. *Polish Polar Research*, 30: 161–178.

Kabała, C. & Zapart, J., 2012. Initial soil development and carbon accumulation on moraines of the rapidly retreating Werenskiold Glacier, SW Spitsbergen, Svalbard archipelago. *Geoderma*, 175–176: 9–12.

Kieres, A. & Piestrzyński, A., 1992. Ore-mineralization of the Hecla Hoek Succession (Precambrian) around Werenskioldbreen, South Spitsbergen. *Studia Geologica Polonica*, 48: 116–151.

Kolondra, L., 2002. *Werenskioldbreen and Surrounding Areas, Spitsbergen, Svalbard, Norway. Orthophotomap 1:25000.* Silesia University, Sosnowiec and Norsk Polarinstitutt, Tromsø.

Krawczyk, W. E., Bartoszewski, S. A. & Siwek, K., 2008. Rain water chemistry at Calypsobyen. *Polish Polar Research*, 29: 149–162.

Lecomte, K. L., Pasquini, A. J & Depetris, P. J., 2005. Mineral weathering in a Semiarid Mountains River: its assessment through inverse modeling. *Aquatic Geochemistry*, 11: 173–194.

Majka, J., Be'eri-Shlevin, Y., Gee, D. G., Czerny, J., Frei, D. & Ladenberger, A., 2013. Torellian (*c.* 640 Ma) metamorphic overprint of the Tonian (*c.* 950 Ma) basement in the Caledonides of southwestern Svalbard. *Geological Magazine*, 151: 732–748.

Majka, J., Czerny, J., Mazur. S., Holm, D. K. & Manecki, M., 2010. Neoproterozoic metamorphic evolution of the Isbjørnhamna Group rocks from south-western Svalbard. *Polar Research*, 29: 250–264.

Majka, J., Mazur, S., Manecki, M., Czerny, J. & Holm, D. K., 2008. Late Neoproterozoic amphibolite facies metamorphism of a pre-Caledonian basement block in southwest Wedel Jarlsberg Land, Spitsbergen: new evidence from U-Th-Pb dating of monazite. *Geological Magazine*, 145: 822–830.

Manecki, M., Holm, D. K., Czerny, J. & Lux, D., 1998. Thermochronological evidence for late Proterozoic (Vendian) cooling in southwest Wedel Jarlsberg Land, Spitsbergen. *Geological Magazine*, 135: 63–69.

Marsz, A. A. & Styszyńska, A., 2007. *The Climate in the Vicinity of Polish Polar Station in Hornsund.* Akademia Morska, Gdynia, 376 pp.

Mehra, O. P. & Jackson, M. L., 1960. Iron oxide removal from soils and clays by a dithionite-citrate system buffered with sodium carbonate. *Clays and Clay Minerals*, 7: 317–327.

Murakami, T., Isobe, H., Sato, T. & Ohnuki., T., 1996. Weathering of chlorite in a quartz-chlorite schist. I. Mineralogical and chemical changes. *Clays and Clay Minerals*, 44: 244–256.

Nemergut, D. R., Anderson, S. P., Cleveland, C. C., Martin, A. P. & Miller, A. E., 2007. Microbial community succession in an unvegetated, recently deglaciated soil. *Microbial* Ecology, 53: 110–122.

Parkhurst, D. L., 1995. *User's guide to PHREEQC – a computer program for speciation, reaction-path, advective-transport and inverse geochemical calculations.* US Geological Survey Water Resources Investigation Report 95–4227, 143 pp.

Pälli, A., Moore, J. C., Jania, J., Kolondra, L. & Głowacki, P., 2003. The drainage pattern of Hansbreen and Werenskioldbreen, two polythermal glaciers in Svalbard. *Polar Re-*

search, 22: 355–371.

Schwertmann, U., 1985. The effect of pedogenic environments on iron oxide minerals. *Advances in Soil Science*, 1: 172–200.

Sigler, W. V. & Zeyer, J., 2002. Microbial diversity and activity along the forefields of two receding glaciers. *Microbial Ecology*, 43: 397–407.

Skiba, S., Drewnik, M. & Kacprzak, A., 2002. Soil of the western coast of Sörkappland. In: Ziaja, W. & Skiba, S. (eds), *Sörkappland Landscape Structure and Functioning (Spitsbergen, Svalbard).* Wydawnictwo Uniwersytetu Jagiellońskiego, Kraków, pp. 51–86.

Straneo, F. & Heimbach, P., 2013. North Atlantic warming and the retreat of Greenland's outlet glaciers. *Nature*, 504: 36–43.

Szynkiewicz, A., Modelska, M., Buczyński, S., Borrok, D. M. & Merrison, J. P., 2013. The polar sulfur cycle in the Werenskioldbreen, Spitsbergen: Possibile implications for understanding the deposition of sulfate minerals in the North Polar Regions of Mars. *Geochimica et Cosmochimica Acta*, 106: 326–343.

Taylor, A. & Blum, J. D., 1995. Relation between soil age and silicate weathering rates determined from the chemical evolution of a glacial chronosequence. *Geology*, 23: 979–982.

Tranter, M., Sharp, M. J., Lamb, H. R., Brown, G. H., Hubbard, B. P. & Willis, I. C., 2002. Geochemical weathering at the bed of Haut Glacier d'Arolla, Switzerland – a new model. *Hydrological Processes*, 16: 959–993.

Van Reeuwijk, L. P., 2006*. Procedures for Soil Analysis. Technical Report, 7th edition.* ISRiC – World Soil Information Centre, Wageningen, the Netherlands, 118 pp.

Wadham, J. L., Cooper, R. J., Tranter, M. & Bottrell, S., 2007. Evidence for widespread anoxia in the proglacial zone of an Arctic glacier. *Chemical Geology*, 243: 1–15.

Wadham, J. L., Cooper, R. J., Tranter, M. & Hodgkins, R., 2001. Enhancement of glacial solute fluxes in the proglacial zone of a polythermal glacier. *Journal of Glaciology*, 47: 378–386.

Wadham, J. L., Hodson, A. J., Tranter, M. & Dowdeswell, J. A., 1997. The rate of chemical weathering beneath a quiescent, surge type, polythermal-based glacier, southern Spitsbergen. *Annales of Glaciology*, 24: 27–31.

White, A. F., 2003. Natural weathering rates of silicate minerals. *Treatise on Geochemistry,* 5: 133–168.

White, A. F. & Brantley, S. L., 2003. The effect of time on the weathering of silicate minerals: why do weathering rates differ in the laboratory and field? *Chemical Geology*, 202: 479–506.

Wilson, M. J., 2004. Weathering of the primary rock-forming minerals: processes, products and rates. *Clay Minerals*, 39: 233–266.

Yoshitake, S., Uchida, M., Koizumi, H. & Nakatsubo, T., 2007. Carbon and nitrogen limitation of soil microbial respiration in a high arctic successional glacier foreland near Ny-Alesund, Svalbard. *Polar Research*, 26: 22–30.

Zhu, C., 2005. In situ feldspar dissolution rates in an aquifer. *Geochimica et Cosmochimica Acta*, 69: 1435–1453.